

Coupling between heavy fermion superconductor CeCoIn₅ and antiferromagnetic metal CeIn₃ through the atomic interface

M. Naritsuka,* S. Nakamura, Y. Kasahara, T. Terashima, R. Peters, and Y. Matsuda†
Department of Physics, Kyoto University, Kyoto 606-8502, Japan
 (Dated: April 8, 2024)

To study the mutual interaction between unconventional superconductivity and magnetic order through an interface, we fabricate hybrid Kondo superlattices consisting of alternating layers of the heavy-fermion superconductor CeCoIn₅ and the antiferromagnetic (AFM) heavy-fermion metal CeIn₃. The strength of the AFM fluctuations is tuned by applying hydrostatic pressure to the CeCoIn₅(*m*)/CeIn₃(*n*) superlattices with *m* and *n* unit-cell-thick layers of CeCoIn₅ and CeIn₃, respectively. The superconductivity in CeCoIn₅ and the AFM order in CeIn₃ coexist in spatially separated layers in the whole thickness and pressure ranges. At ambient pressure, the Néel temperature T_N of the CeIn₃ block layers (BLs) of CeCoIn₅(7)/CeIn₃(*n*) shows little dependence on the thickness *n*, in sharp contrast to CeIn₃(*n*)/LaIn₃(4) superlattices where T_N is strongly suppressed with decreasing *n*. This suggests that each CeIn₃ BL is magnetically coupled by the RKKY interaction through the adjacent CeCoIn₅ BL and a three-dimensional magnetic state is formed. With applying pressure to CeCoIn₅(7)/CeIn₃(13), T_N of the CeIn₃ BLs is suppressed up to 2.4 GPa, showing a similar pressure dependence as bulk CeIn₃ single crystals. An analysis of the upper critical field reveals that the superconductivity in the CeCoIn₅ BLs is barely influenced by the AFM fluctuations in the CeIn₃ BLs, even when the CeIn₃ BLs are in the vicinity of the AFM quantum critical point. This is in stark contrast to CeCoIn₅/CeRhIn₅ superlattices, in which the superconductivity in the CeCoIn₅ BLs is profoundly affected by AFM fluctuations in the CeRhIn₅ BLs. The present results show that although AFM fluctuations are injected into the CeCoIn₅ BLs from the CeIn₃ BLs through the interface, they barely affect the force which binds superconducting electron pairs. These results demonstrate that two-dimensional AFM fluctuations are essentially important for the pairing interactions in CeCoIn₅.

I. INTRODUCTION

It is well established that in several compound families, such as high- T_c cuprates, iron pnictides/chalcogenides, and heavy-fermion compounds, Cooper pairs are not bound together through phonon exchange but instead through exchange of some other kind, such as spin fluctuations^{1–8}. Despite tremendous efforts, however, the interplay between unconventional superconductivity and magnetism still remains largely unexplored in these systems. This includes fascinating electronic phases, where superconductivity and antiferromagnetic (AFM) order, involving the same charge carriers, coexists, and the important question why superconductivity is often strongest near a quantum critical point (QCP) where the AFM order vanishes in the zero temperature limit and spin fluctuations become singular^{9–13}.

By using a recent state-of-the-art molecular beam epitaxy (MBE) technique, we grow artificial Kondo superlattices with alternating layers of heavy-fermion superconductors and conventional metals or heavy-fermion AFM compounds^{14,15}. These Kondo superlattices provide unique opportunity to study the mutual interactions between the unconventional superconducting state and magnetically ordered- or conventional metallic-states through the atomic interface and thereby seek answers to the above-mentioned questions. Until now, several types of Kondo superlattices containing the heavy-fermion superconductor CeCoIn₅¹⁶ with a layered structure have been fabricated^{17–22}. CeCoIn₅ has a quasi-two dimen-

sional (2D) Fermi surface²³ and the presence of quasi-2D AFM fluctuations has been reported in the normal state^{24,25}. Furthermore, a superconducting gap with $d_{x^2-y^2}$ -wave symmetry has been observed by a variety of experiments^{26–31}. The superconducting state is strongly Pauli limited, as demonstrated by a first-order phase transition at upper critical fields for directions parallel and perpendicular to the *ab* plane^{26,32–34}. It is a prototypical system, in which non-Fermi liquid behaviors in the normal state and unconventional superconductivity are thought to arise from the proximity to a AFM QCP^{35–37}. Under pressure, CeCoIn₅ moves away from the QCP and Fermi liquid behavior is recovered.

It has been shown that in superlattices consisting of alternating layers of CeCoIn₅ and the conventional metal YbCoIn₅ with atomic layer thicknesses (Fig. 1a), the Pauli pair-breaking effect is strongly suppressed from that in the bulk of CeCoIn₅ single crystals^{18,19}. Site-selective nuclear magnetic resonance (NMR) measurements on CeCoIn₅/YbCoIn₅ superlattices have reported that AFM fluctuations in the CeCoIn₅ block layers (BLs), particularly in the vicinity of the interface, are weakened³⁸. These results have been attributed to the local inversion symmetry breaking at the interface, which results in spin-split Fermi surfaces and thus effectively suppresses the Zeeman effect^{18,19,39}.

In superlattices consisting of alternating layers of CeCoIn₅ and the heavy-fermion AFM metal CeRhIn₅ (Fig. 1b), the superconducting- and AFM-states coexist in spatially separated layers. In these superlattices, the influence of the local inversion symmetry break-

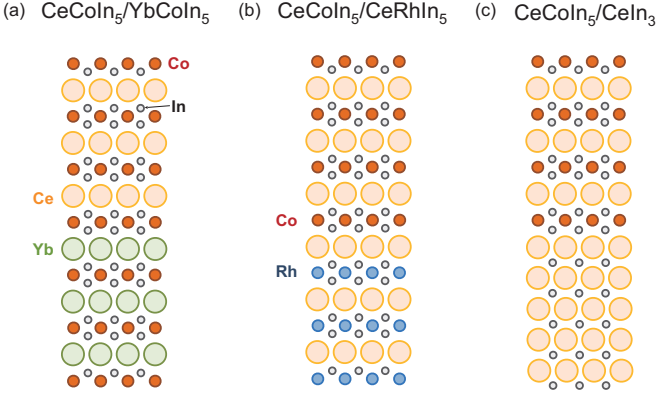


FIG. 1. Schematic representations of three types of Kondo superlattices, (a) $\text{CeCoIn}_5/\text{YbCoIn}_5$ (b) $\text{CeCoIn}_5/\text{CeRhIn}_5$, and (c) $\text{CeCoIn}_5/\text{CeIn}_3$, where CeCoIn_5 is a heavy-fermion d -wave superconductor, YbCoIn_5 is a conventional metal, and CeRhIn_5 and CeIn_3 are heavy-fermion AFM metals. The atomic views of the $[100]$ plane are shown.

ing at the interface has been shown to be less important compared to $\text{CeCoIn}_5/\text{YbCoIn}_5$. In sharp contrast to $\text{CeCoIn}_5/\text{YbCoIn}_5$, NMR measurements have revealed that magnetic fluctuations in CeCoIn_5 BLs of $\text{CeCoIn}_5/\text{CeRhIn}_5$ superlattices are enhanced compared to bulk CeCoIn_5 single crystal, highlighting the importance of the magnetic proximity effect⁴⁰. In particular, it has been pointed out that in the vicinity of the QCP of CeRhIn_5 BLs, AFM fluctuations are enhanced and the force binding superconducting electron-pairs acquires an extremely strong-coupling nature. This indicates that superconducting pairing can be manipulated by magnetic fluctuations injected through the interface²².

To obtain further insight into the mutual interactions between unconventional superconductivity and magnetic order, we here fabricate superlattices consisting of alternating layers of CeCoIn_5 and the AFM metal CeIn_3 (Fig. 1c). CeIn_3 is an isotropic Kondo lattice material with cubic crystal structure. In bulk CeIn_3 single crystals, AFM order with ordered magnetic moment of $0.48\mu_B$ occurs at $T_N=10\text{ K}$, where μ_B is the Bohr magneton⁴¹. With applying pressure, T_N decreases and vanishes at $\sim 2.6\text{ GPa}$, indicating an AFM QCP. Superconductivity with a maximum $T_c \approx 200\text{ mK}$ is induced in a very narrow pressure range around the QCP^{9,42}.

Our results reveal that, similar to $\text{CeCoIn}_5/\text{CeRhIn}_5$ but in contrast to $\text{CeCoIn}_5/\text{YbCoIn}_5$ superlattices, the local inversion symmetry breaking at the interface has only little effect on the superconductivity in $\text{CeCoIn}_5/\text{CeIn}_3$ superlattices. However, we find that the magnetic and the superconducting properties in $\text{CeCoIn}_5/\text{CeIn}_3$ are in marked contrast to those in $\text{CeCoIn}_5/\text{CeRhIn}_5$ superlattices²². Although the AFM fluctuations are injected to the CeCoIn_5 BLs from the CeIn_3 BLs through the interfaces, they barely affect the electron pairing interactions in the CeCoIn_5 BLs. These

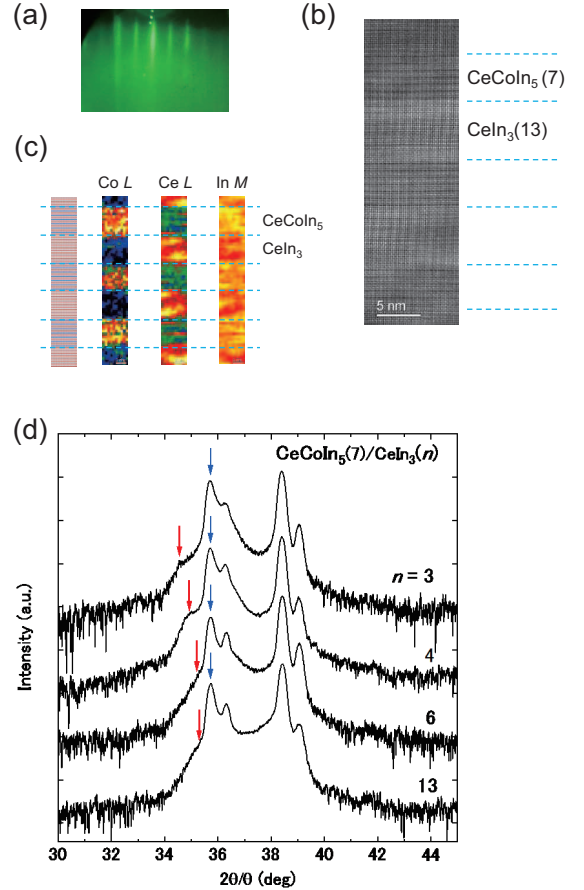


FIG. 2. (a) Typical RHEED streak patterns for $\text{CeCoIn}_5(7)/\text{CeIn}_3(13)$ superlattice taken during the crystal growth. (b), (c) High-resolution cross-sectional (b) TEM image and (c) EELS images for the $\text{CeCoIn}_5(7)/\text{CeIn}_3(13)$ superlattice with the electron beam aligned along the (100) direction. The EELS images were taken for Co L , Ce L , and In M edges. (d) $\text{Cu } K\alpha_1$ x-ray diffraction patterns for $\text{CeCoIn}_5(7)/\text{CeIn}_3(n)$ superlattices ($n=3, 4, 6$, and 13). The blue and red arrows indicate the $[003]$ peaks of CeCoIn_5 and satellite peaks due to the superlattice structure, respectively.

results provide compelling evidence that 2D AFM fluctuations are essentially important for the superconductivity in CeCoIn_5 .

II. EXPERIMENTAL DETAILS

The hybrid superlattices $\text{CeCoIn}_5(7)/\text{CeIn}_3(n)$ ($n=3, 4, 6$ and 13) with c axis oriented structure are grown on a MgF_2 substrate by MBE technique^{14,15}. We first grow ~ 20 unit-cell-thick (UCT) CeIn_3 ($\sim 10\text{ nm}$) as a buffer layer on MgF_2 . Then 7-UCT CeCoIn_5 and n -UCT CeIn_3 ($n=3, 4, 6$ and 13) are grown alternatively with total thicknesses of approximately 200 nm . As the epitaxial growth temperature of CeCoIn_5 and CeIn_3 layers are different, CeCoIn_5 and CeIn_3 BLs were grown at 570

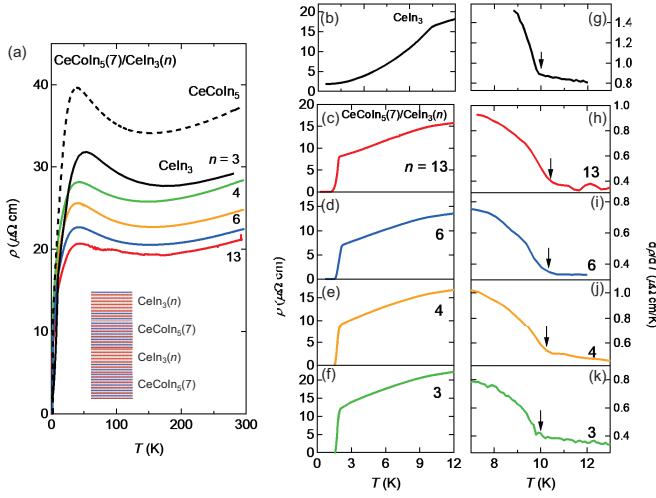


FIG. 3. (a) Temperature dependence of the resistivity $\rho(T)$ in $\text{CeCoIn}_5(7)/\text{CeIn}_3(n)$ superlattices for $n=3, 4, 6$, and 13 , along with $\rho(T)$ for CeIn_3 and CeCoIn_5 thin films. Inset illustrates the schematics of $\text{CeCoIn}_5(7)/\text{CeIn}_3(n)$ superlattice. (b)-(f) $\rho(T)$ at low temperatures. (g)-(k) Temperature derivative of the resistivity, $d\rho(T)/dT$, as a function of temperature. The arrows indicate the Néel temperature T_N .

and 420°C , respectively. The superlattice is capped with $\sim 5\text{ nm}$ Co to prevent oxidation. Streak pattern of the reflection high-energy electron diffraction (RHEED) image shown in Fig. 2(a) have been observed during the whole growth of the superlattices, indicating good epitaxy. The atomic force microscope measurements reveal that the surface roughness is within $\pm 1\text{ nm}$, which is comparable to 1-2 UCT along the c axis of the constituents. Because atomically flat regions extend over distances of $\sim 0.1\text{ }\mu\text{m}$, it can be expected that transport properties are not seriously influenced by the roughness. Figure 2(b) displays a high-resolution cross-sectional transmission electron microscope (TEM) image along the (100) direction for the $\text{CeCoIn}_5(7)/\text{CeIn}_3(13)$ superlattice. A clear interface between the CeCoIn_5 and the CeIn_3 layers is observed. Figure 2(c) displays an electron energy loss spectroscopy (EELS) image of the same superlattice. The EELS images clearly resolve the 7-UCT CeCoIn_5 and the 13-UCT CeIn_3 BLs, demonstrating sharp interfaces with no atomic interdiffusion between the neighboring CeCoIn_5 and CeIn_3 BLs. Figure 2(d) shows the X-ray diffraction patterns for $\text{CeCoIn}_5/\text{CeIn}_3(n)$ superlattices. The shoulder structure shown by the red arrows near the $[003]$ peak of CeCoIn_5 (blue arrows) is consistent with the superlattice structure. These results demonstrate the successful fabrication of epitaxial superlattices with sharp interfaces. High-pressure resistivity measurements have been performed under pressure up to 2.4 GPa using a piston cylinder cell with Daphne oil 7373 as the pressure transmitting medium. The pressure has been measured by the T_c of Pb.

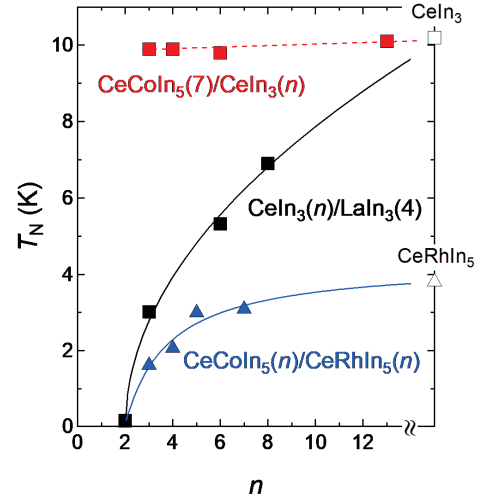


FIG. 4. The Néel temperature T_N for $\text{CeCoIn}_5(7)/\text{CeIn}_3(n)$ as a function of n . For comparison, T_N for $\text{CeIn}_3(n)/\text{LaIn}_3(4)$ and $\text{CeCoIn}_5(n)/\text{CeRhIn}_5(n)$ are shown. Open square and triangle are T_N of bulk CeIn_3 and CeRhIn_5 single crystals, respectively.

III. RESULTS

Figure 3(a) depicts the temperature dependence of the resistivity ρ of $\text{CeCoIn}_5(7)/\text{CeIn}_3(n)$ superlattices with $n=3, 4, 6$ and 13 . We also show ρ of CeCoIn_5 and CeIn_3 thin films grown by MBE. The resistivity of $\text{CeCoIn}_5(7)/\text{CeIn}_3(n)$ superlattices follows the typical heavy-fermion behavior. With decreasing temperature, $\rho(T)$ increases below $\sim 150\text{ K}$ due to the Kondo scattering but then begins to decrease due strong c - f hybridization between f -electrons and conduction (c) band electrons, leading to the narrow f -electron band at the Fermi level. Figures 3(b)-3(f) depict $\rho(T)$ at low temperatures. All superlattices show the superconducting transition at $\approx 1.5\text{ K}$. For the $n=3$ - and 4 -superlattices, $\rho(T)$ exhibit a slight downward curvature. Figures 3(g)-3(k) display the temperature derivative of the resistivity $d\rho(T)/dT$. As shown by the arrows in Fig. 3(g), $d\rho(T)/dT$ of CeIn_3 thin film exhibits a distinct kink at $T_N=10\text{ K}$ ⁴¹. Similar kink structures are observed in all superlattices at the temperatures indicated by arrows, showing the AFM transition.

Figure 4 shows the thickness dependence of T_N of the $\text{CeCoIn}_5(7)/\text{CeIn}_3(n)$ superlattices. For comparison, the data sets of $\text{CeIn}_3(4)/\text{LaIn}_3(n)$, where LaIn_3 is a non-magnetic conventional metal with no f -electrons¹⁴, and $\text{CeCoIn}_5(n)/\text{CeRhIn}_5(n)$ are also included in the figure. Remarkably, the observed thickness dependence of T_N in $\text{CeCoIn}_5/\text{CeIn}_3$ is in striking contrast to that in $\text{CeIn}_3/\text{LaIn}_3$; While T_N is strongly suppressed with decreasing n and vanishes at $n=2$ in $\text{CeIn}_3/\text{LaIn}_3$, T_N is nearly independent of n in $\text{CeCoIn}_5(7)/\text{CeIn}_3(n)$. This suggests that CeIn_3 BLs are coupled weakly by the Ruderman-Kittel-Kasuya-Yosida (RKKY) interac-

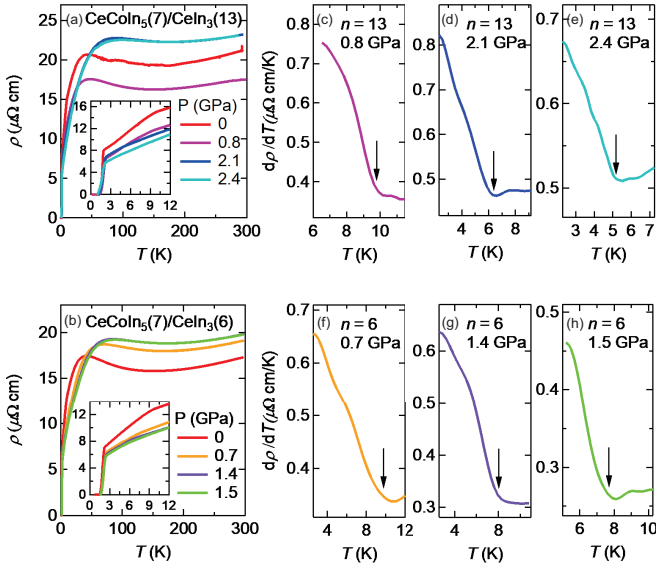


FIG. 5. (a), (e) Temperature dependence of the resistivity $\rho(T)$ under pressure for $\text{CeCoIn}_5(7)/\text{CeIn}_3(n)$ for (a) $n=13$ and (e) $n=6$. Inset: $\rho(T)$ at low temperatures. (b)-(d) and (f)-(h) show the temperature derivative of the resistivity, $d\rho(T)/dT$, as a function of temperature under pressure for $n=13$ and $n=6$, respectively. The arrows indicate the Néel temperature T_N .

tions through the adjacent LaIn_3 BL, but they can strongly couple through the adjacent CeCoIn_5 BL. This is even more surprising, as the distance between different CeIn_3 BLs is larger in the $\text{CeCoIn}_5(7)/\text{CeIn}_3(n)$ superlattices than in the $\text{CeIn}_3(n)/\text{LaIn}_3(4)$ superlattices. We thus conclude that small but finite magnetic moments are induced in CeCoIn_5 BLs in $\text{CeCoIn}_5/\text{CeIn}_3$, which mediate the RKKY-interaction. On the other hand, because of the absence of strongly interacting f -electrons in LaIn_3 , which can form magnetic moments, the RKKY interaction in $\text{CeIn}_3/\text{LaIn}_3$ can be expected to be much weaker. To clarify this, a microscopic probe of magnetism, such as NMR measurements, is required. We note that as shown in Fig. 4, the reduction of T_N is also observed in $\text{CeCoIn}_5(n)/\text{CeRhIn}_5(n)$ superlattices²², suggesting that the RKKY interaction between CeRhIn_5 BLs through adjacent CeCoIn_5 BL is negligibly small. This is supported by the recent site-selective NMR measurements which report no discernible magnetic moments induced in the CeCoIn_5 BLs in $\text{CeCoIn}_5/\text{CeRhIn}_5$ ⁴⁰.

The pressure dependence of the superconducting and magnetic properties provide crucial information on the mutual interaction between superconductivity and magnetism through the interface. Figures 5(a) and 5(b) and their insets show the temperature dependence of $\rho(T)$ under pressure for $\text{CeCoIn}_5(7)/\text{CeIn}_3(n)$ for $n=13$ and 6, respectively. With the application of pressure, the temperature at which $\rho(T)$ shows its maximum increases due to the enhancement of the c - f hybridization³⁶. As

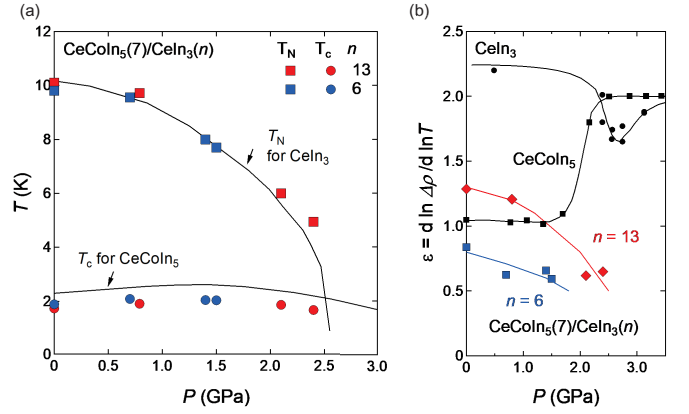


FIG. 6. (a) Pressure dependence of T_N and T_c of $\text{CeCoIn}_5(7)/\text{CeIn}_3(n)$ superlattices for $n=13$ and 6. For comparison, T_N of CeIn_3 and T_c of CeCoIn_5 single crystals are shown by solid lines. (b) Pressure dependence of the exponent ε in $\rho(T) = \rho_0 + AT^\varepsilon$, obtained from $d \ln \Delta\rho / d \ln T$ ($\Delta\rho = \rho(T) - \rho_0$), for the $\text{CeCoIn}_5(7)/\text{CeIn}_3(n)$ superlattices for $n=13$ and 6. For comparison, ε for bulk CeIn_3 and CeCoIn_5 single crystals is shown.

shown in the insets, both superlattices undergo a superconducting transition under pressure. Figures 5(c)-5(e) and 5(f)-5(h) show $d\rho(T)/dT$ under pressure for $n=13$ and 6, respectively. Clear kink structure associated with the AFM transition can be seen in the data.

Figure 6(a) depicts the pressure dependence of T_N and T_c for $\text{CeCoIn}_5(7)/\text{CeIn}_3(n)$ superlattices for $n=6$ and 13. With applying pressure, T_N decreases rapidly. For comparison, T_N of a bulk single crystal CeIn_3 is also shown by the solid line⁹. The pressure dependence of T_N of both superlattices are very similar to that of the bulk CeIn_3 single crystal. In bulk CeIn_3 crystal, the AFM QCP is located at $p_c \approx 2.6$ GPa. It is natural to expect, therefore, that the AFM QCP of the superlattices is close to 2.6 GPa. Thus, at 2.4 GPa, the superlattices are in the vicinity of the AFM QCP. This is supported by the temperature dependence of the resistivity under pressure. The resistivity can be fitted as

$$\rho(T) = \rho_0 + AT^\varepsilon. \quad (1)$$

Figure 6(b) shows the pressure dependence of ε obtained from $d \ln \Delta\rho / d \ln T$, where $\Delta\rho = \rho(T) - \rho_0$. The magnitude of ε decreases with pressure. In bulk CeIn_3 single crystal, ε decreases with pressure and exhibits a minimum at the AFM QCP^{9,42}. On the other hand, applying pressure to CeCoIn_5 leads to an increase of ε , which is attributed to the suppression of the non-Fermi liquid behavior, $\rho(T) \propto T$, and the development of a Fermi liquid state with its characteristic $\rho(T) \propto T^2$ dependence^{35,36}. Therefore, the reduction of ε with pressure arises from the CeIn_3 BLs, indicating that the CeIn_3 BLs approach the AFM QCP.

As shown in Fig. 6(a), T_c increases, peaks at ~ 1.8 GPa, and then decreases when applying pressure. This pres-

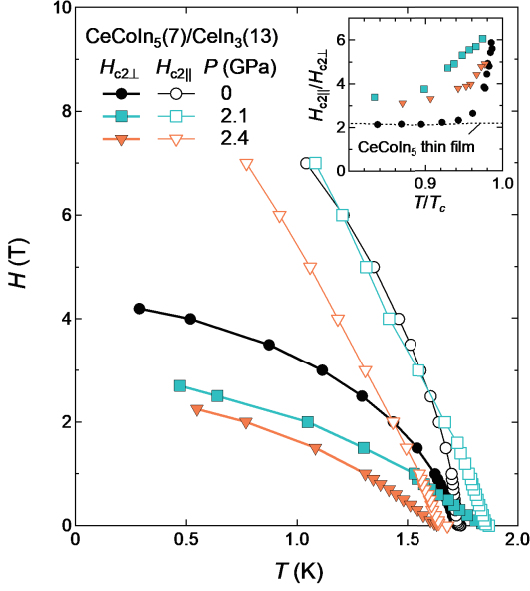


FIG. 7. Temperature dependence of upper critical fields in magnetic fields parallel ($H_{c2||}$, open symbols) and perpendicular ($H_{c2\perp}$, closed symbols) to the ab -plane for $\text{CeCoIn}_5(7)/\text{CeIn}_3(13)$ superlattice at ambient pressure and at 2.1 and 2.4 GPa. The inset shows anisotropy of the upper critical field, $H_{c2||}/H_{c2\perp}$. The data of CeCoIn_5 thin film at ambient pressure is shown by dotted line.

sure dependence bears resemblance to that of CeCoIn_5 bulk single crystals³⁵. An analysis of the upper critical field provides important information about the superconductivity of CeCoIn_5 BLs. Figure 7 depicts the temperature dependence of the upper critical field determined by the midpoint of the resistive transition in a magnetic field \mathbf{H} applied parallel ($H_{c2||}$) and perpendicular ($H_{c2\perp}$) to the layers. The inset of Fig. 7 shows the anisotropy of the upper critical fields $H_{c2||}/H_{c2\perp}$ at ambient pressure. The anisotropy diverges on approaching T_c . This is in sharp contrast to the CeCoIn_5 thin film, whose anisotropy is nearly temperature independent up to T_c . The observed diverging anisotropy indicates that the superconducting electrons are confined in the 2D CeCoIn_5 BLs. In fact, in 2D superconductivity, $H_{c2||}$ is limited by Pauli paramagnetic pair breaking and increases as $\sqrt{T_c - T}$, while $H_{c2\perp}$ increases as $T_c - T$ due to the orbital pair breaking near T_c ¹⁷. Moreover, the thickness of the CeCoIn_5 BL is comparable to the coherence length perpendicular to the layer, $\xi_c \sim 4$ nm. Thus each 7-UCT CeCoIn_5 BL effectively behaves as a 2D superconductor.

IV. DISCUSSION

It has been revealed that the temperature dependence of $H_{c2\perp}$ provides crucial information about the impact of the interface on the superconductivity in CeCoIn_5 BLs. In particular, the modification of the Pauli para-

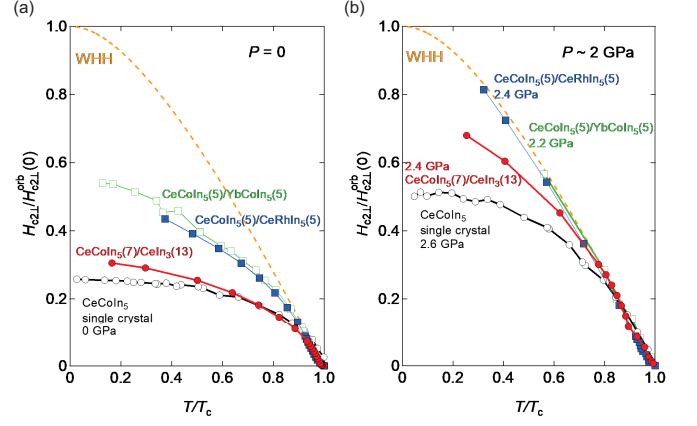


FIG. 8. (a) Upper critical field in perpendicular field normalized by the orbital limiting upper critical field, $H_{c2\perp}/H_{c2\perp}^{orb}(0)$, plotted as a function of T/T_c (a) at ambient pressure and (b) under pressure about 2 GPa for $\text{CeCoIn}_5(7)/\text{CeIn}_3(13)$ superlattices. For comparison, $H_{c2\perp}/H_{c2\perp}^{orb}(0)$ for bulk CeCoIn_5 single crystal, $\text{CeCoIn}_5(5)/\text{YbCoIn}_5(5)$ and $\text{CeCoIn}_5(5)/\text{CeRhIn}_5(5)$ are shown. Orange dotted lines represent the WHH curve, which is upper critical field for purely orbital limiting.

magnetic effect in the superlattice, which dominates the pair breaking in bulk CeCoIn_5 single crystals, gives valuable clues^{18,19,21,22}. Figure 8(a) and 8(b) depict the T dependence of the $H_{c2\perp}$ of $\text{CeCoIn}_5(7)/\text{CeIn}_3(13)$ superlattice, normalized by the orbital-limited upper critical field at zero temperature, $H_{c2\perp}^{orb}(0)$, which is obtained from the Werthamer-Helfand-Hohenberg (WHH) formula, $H_{c2\perp}^{orb}(0) = -0.69T_c(dH_{c2\perp}/dT)_{T_c}$ ⁴³. In Figs. 8(a) and 8(b), two extreme cases are also included; the WHH curve with no Pauli pair-breaking and $H_{c2}/H_{c2\perp}^{orb}(0)$ for bulk CeCoIn_5 single crystal³². For comparison, $H_{c2\perp}^{orb}(0)$ for $\text{CeCoIn}_5/\text{YbCoIn}_5$ and $\text{CeCoIn}_5/\text{CeRhIn}_5$ are also shown^{17,22}.

At ambient pressure, $H_{c2\perp}/H_{c2\perp}^{orb}(0)$ of $\text{CeCoIn}_5/\text{YbCoIn}_5$ and $\text{CeCoIn}_5/\text{CeRhIn}_5$ are strongly enhanced from that of CeCoIn_5 bulk single crystals, indicating the suppression of the Pauli paramagnetic pair-breaking effect. However, it has been pointed out that the mechanisms of this suppression in these two systems are essentially different. In $\text{CeCoIn}_5/\text{YbCoIn}_5$, the enhancement of $H_{c2\perp}/H_{c2\perp}^{orb}(0)$ is caused by the local inversion symmetry breaking at the interface^{18,39}. The asymmetry of the potential perpendicular to the 2D plane of the superlattice, $\nabla V \parallel [001]$, induces the Rashba spin-orbit interaction $\alpha_R = \mathbf{g}(\mathbf{k}) \cdot \boldsymbol{\sigma} \propto (\mathbf{k} \times \nabla V) \cdot \boldsymbol{\sigma}$, where $\mathbf{g}(\mathbf{k}) = (k_y, -k_x, 0)/k_F$, k_F and $\boldsymbol{\sigma}$ are the Fermi wave number and the Pauli matrices, respectively. The Rashba spin-orbit interaction splits the Fermi surface into two sheets with different spin textures⁴⁴. The energy splitting is given by α_R , and the spin direction is tilted into the 2D plane, rotating clockwise on one sheet and anticlockwise on the other. When the Rashba splitting exceeds the superconducting gap energy ($\alpha_R > \Delta$), the

superconducting state is dramatically modified^{39,44,45}. In particular, when the magnetic field is applied perpendicular to the 2D plane, the magnetic field does not couple to the spins, leading to a suppression of the Pauli pair-breaking effect. At $p=2.2$ GPa, $H_{c2\perp}/H_{c2\perp}^{orb}(0)$ of CeCoIn₅/YbCoIn₅ nearly coincides with the WHH curve. This indicates that $H_{c2\perp}$ is dominated by the orbital pair breaking most likely due to the suppression of the Pauli paramagnetic pair-breaking effect by the Rashba splitting.

On the other hand, in CeCoIn₅/CeRhIn₅ superlattices, it has been shown that the effect of the local inversion symmetry breaking on $H_{c2\perp}$ is less important compared with CeCoIn₅/YbCoIn₅²². It has been proposed that magnetic fluctuations (paramagnons) in CeRhIn₅ BLs injected through the interface dramatically enhance the force binding superconducting electron pairs in CeCoIn₅ BLs, leading to the enhancement of Δ . As a result, the Pauli limiting field $H_{c2\perp}^{Pauli}(= \sqrt{2}\Delta/g\mu_B)$ is enhanced, where g is the g -factor of the electrons. This increases the relative importance of the orbital pair-breaking effect, giving rise to the enhancement of $H_{c2\perp}/H_{c2\perp}^{orb}(0)$ ²². At $p=2.1$ GPa, which is close to the AFM QCP of CeRhIn₅ BLs, $H_{c2\perp}/H_{c2\perp}^{orb}(0)$ nearly coincides with the WHH curve. This has been attributed to the enhanced Pauli limiting field that well exceeds the orbital limiting field ($H_{c2\perp}^{Pauli} \gg H_{c2\perp}^{orb}$)²².

In contrast to CeCoIn₅/YbCoIn₅ and CeCoIn₅/CeRhIn₅, $H_{c2\perp}/H_{c2\perp}^{orb}(0)$ is only slightly enhanced in CeCoIn₅(7)/CeIn₃(13) superlattice at ambient pressure from that of bulk CeCoIn₅ single crystal. This indicates that $H_{c2\perp}$ is dominated by Pauli paramagnetic effect, i.e. $H_{c2\perp} \approx H_{c2\perp}^{Pauli} \ll H_{c2\perp}^{orb}$. This implies that the effect of local inversion symmetry breaking on the superconductivity in CeCoIn₅/CeIn₃ is weak compared with CeCoIn₅/YbCoIn₅. The local inversion symmetry is broken for the CeCoIn₅/YbCoIn₅ on the CoIn-layer while it is broken on the Ce layer for CeCoIn₅/CeIn₃ and CeCoIn₅/CeRhIn₅. Therefore, the present results suggest that the inversion symmetry breaking on the CoIn-layer induces a larger local electric field gradient. Moreover, superconducting electrons in CeCoIn₅ BLs are not strongly influenced by the AFM order in CeIn₃ BLs compared with CeCoIn₅/CeRhIn₅.

When superconductivity is dominated by the Pauli-limiting effect ($H_{c2\perp} \approx H_{c2\perp}^{Pauli}$), $2\Delta/k_B T_c$ is estimated as

$$\frac{2\Delta}{k_B T_c} \approx \sqrt{2} \frac{g\mu_B H_{c2\perp}}{k_B T_c}. \quad (2)$$

Figure 9 depicts the pressure dependence of $q = \sqrt{2}g\mu_B H_{c2\perp}/k_B T_c$ for CeCoIn₅/CeRhIn₅ and CeCoIn₅/CeIn₃, along with q for bulk CeCoIn₅ single crystal. Here $g=2$ is assumed. We note that $q = 4.2$ of the bulk CeCoIn₅ is smaller than the value determined by the specific heat measurements $2\Delta/k_B T_c \approx 6$ ¹⁶, but is larger than the BCS value of $q = 3.54$, which is consistent with the strong coupling superconductivity.

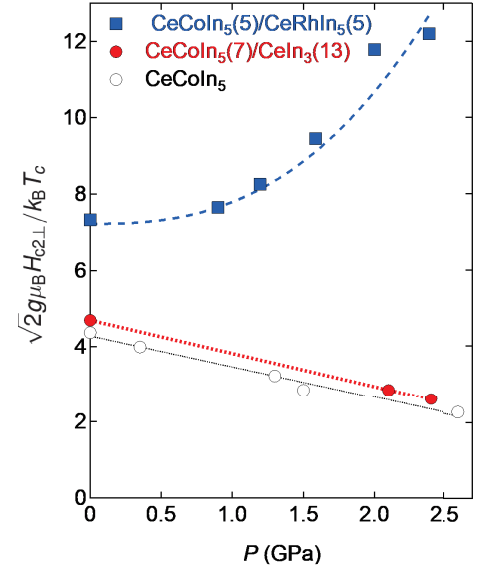


FIG. 9. Pressure dependence of $q = \sqrt{2}g\mu_B H_{c2\perp}/k_B T_c \approx 2\Delta/k_B T_c$ for CeCoIn₅(7)/CeIn₃(13) superlattice. For comparison, q of bulk CeCoIn₅ single crystal and CeCoIn₅(5)/CeRhIn₅(5) are plotted.

The increase of q with pressure in CeCoIn₅/CeRhIn₅ implies the increase of $2\Delta/k_B T_c$. This increase has been attributed to an enhancement of the force binding superconducting electron pairs. In spin fluctuation mediated superconductors, the pairing interaction is mainly provided by high-energy fluctuations while low-energy fluctuations act as pair breaking. In this case, an increase of $2\Delta/k_B T_c$ occurs without accompanying a large enhancement of T_c , which is consistent with the results of CeCoIn₅/CeRhIn₅²². Thus, the critical AFM fluctuations that develop in CeRhIn₅ BLs near the QCP are injected into the CeCoIn₅ BLs through the interface and strongly enhance the pairing interaction in CeCoIn₅ BLs.

In stark contrast to CeCoIn₅/CeRhIn₅ superlattices, q decreases with pressure in bulk CeCoIn₅ single crystal. This implies that the pairing interaction is weakened with applying pressure, which is consistent with the fact that the pressure moves the system away from the QCP of CeCoIn₅. The reduction of $2\Delta/k_B T_c$ with pressure in bulk CeCoIn₅ single crystals is confirmed by the jump of the specific heat at T_c ⁴⁶. It should be stressed that the pressure dependence of q in CeCoIn₅(7)/CeIn₃(13) is very similar to that of bulk CeCoIn₅. This strongly indicates that the pairing interactions in CeCoIn₅ BLs are barely influenced by AFM fluctuations injected from the adjacent CeIn₃ BLs through the interface even when CeIn₃ BLs are located near the AFM QCP.

The most salient feature in the CeCoIn₅/CeIn₃ superlattices is that the superconductivity of CeCoIn₅ BLs is little affected by the critical AFM fluctuations in CeIn₃ BLs, despite the fact that AFM fluctuations are injected

from the adjacent CeIn_3 BLs into CeCoIn_5 BLs, as evidenced by the AFM order in $\text{CeCoIn}_5/\text{CeIn}_3$ demonstrating that different CeIn_3 BLs are magnetically coupled by the RKKY interaction through adjacent CeCoIn_5 BLs. Even in the vicinity to the AFM QCP of the CeIn_3 BLs, the superconducting state in the CeCoIn_5 BLs is very similar to that of CeCoIn_5 bulk single crystals. This indicates that the AFM fluctuations injected from CeIn_3 BLs do not help to enhance the force binding the superconducting electron pairs in CeCoIn_5 BLs.

This is in stark contrast to $\text{CeCoIn}_5/\text{CeRhIn}_5$, in which the pairing force in CeCoIn_5 BL is strongly enhanced by the AFM fluctuations in CeRhIn_5 BLs²², although the CeRhIn_5 BLs are magnetically only weakly coupled through CeCoIn_5 BLs. We point out that these contrasting behaviors can be attributed to the differences of the magnetic and electronic properties of CeRhIn_5 and CeIn_3 . The magnetic wave vector in the ordered phase of CeIn_3 is commensurate $\mathbf{q}_0=(0.5,0.5,0.5)^{41}$. The evolution of the ordered moment below T_N is consistent with mean field theory. On the other hand, the magnetic wave vector in the ordered phase of CeRhIn_5 is incommensurate $\mathbf{q}_0=(0.5,0.5,0.297)^{47}$. The evolution of the ordered moment below T_N deviates from mean field behavior, likely due to 2D fluctuations. In CeCoIn_5 , AFM fluctuations with wave vector $\mathbf{q}_f=(0.45, 0.45, 0.5)$ are dominant²⁵. Thus, the c axis component of \mathbf{q}_f in CeCoIn_5 is commensurate and has the same value as that of \mathbf{q}_0 in CeIn_3 . On the other hand, the c axis component of \mathbf{q}_0 in CeRhIn_5 is incommensurate and very different from that of \mathbf{q}_0 in CeCoIn_5 .

The equality between the c axis component of \mathbf{q}_f in CeCoIn_5 and \mathbf{q}_0 in CeIn_3 would explain why the magnetic coupling between CeIn_3 BLs through CeCoIn_5 BL is stronger than that between CeRhIn_5 BLs. Thus, AFM order is formed in $\text{CeCoIn}_5(7)/\text{CeIn}_3(n)$ even for small n , for which the AFM order has already vanished in $\text{CeCoIn}_5(n)/\text{CeRhIn}_5(n)$. In magnetically mediated superconductors, the pairing interaction is expected to be strongly wave number dependent. Considering that the quasi-2D Fermi surface of CeCoIn_5 bears a close resemblance to that of CeRhIn_5 and the superconducting pairing state of both compounds is $d_{x^2-y^2}$ ⁴⁸, it is likely that the pairing interaction in both compounds has 2D character and peaks around the same wave number. Furthermore, it has been assumed that 2D magnetic fluctuations are strong in CeRhIn_5 . Thus, superconductivity in the CeCoIn_5 BLs of $\text{CeCoIn}_5(n)/\text{CeRhIn}_5(n)$

is strongly influenced. On the other hand, AFM fluctuations having 3D character in CeIn_3 may not play an important role for the pairing interaction in CeCoIn_5 , resulting in little change of the superconductivity in $\text{CeCoIn}_5/\text{CeIn}_3$.

V. SUMMARY

A state-of-the-art MBE technique has enabled us to fabricate superlattices consisting of different heavy-fermion compounds. These Kondo superlattices provide a unique opportunity to study the mutual interaction between unconventional superconductivity and magnetic order through the atomic interface. In hybrid Kondo superlattice $\text{CeCoIn}_5/\text{CeIn}_3$, the superconductivity in CeCoIn_5 BLs and AFM order in CeIn_3 BLs coexist in spatially separated layers. We find that each CeIn_3 BL is magnetically coupled by the RKKY interaction through adjacent CeCoIn_5 BLs. An analysis of the upper critical field under pressure reveals that the superconductivity in CeCoIn_5 BLs is little influenced even in the presence of abundant AFM fluctuations in the vicinity of the AFM QCP of adjacent CeIn_3 BLs. Thus, although the AFM fluctuations are injected to the CeCoIn_5 BLs from the CeIn_3 BLs through the interfaces, they barely influence the force binding superconducting electron pairs. This is in sharp contrast to $\text{CeCoIn}_5/\text{CeRhIn}_5$, in which the superconductivity in the CeCoIn_5 BLs are strongly influenced by quantum critical AFM fluctuations in CeRhIn_5 BLs.

It has been widely believed that 2D AFM fluctuations are important for the pairing interaction in CeCoIn_5 . However, direct evidence was lacking. The present results provide strong support that 2D AFM fluctuations are essentially important for the unconventional superconductivity in CeCoIn_5 .

ACKNOWLEDGEMENTS

We thank K. Ishida, H. Kontani, and Y. Yanase for fruitful discussions. This work was supported by Grants-in-Aid for Scientific Research (KAKENHI) (Nos. 25220710, 15H02014, 15H02106, 17K18753, 18H05227, 18J10553), and on Innovative Areas ‘Topological Material Science’ (No. JP15H05852) and ‘3D Active-Site Science’ (No. 26105004) from Japan Society for the Promotion of Science (JSPS). M. N. also acknowledges support from a JSPS Fellows.

* naritsuka@scphys.kyoto-u.ac.jp

† matsuda@scphys.kyoto-u.ac.jp

¹ M. Sigrist and K. Ueda, Rev. Mod. Phys. **63**, 239 (1991).

² Superconductivity Volume 1: Conventional and Unconventional Superconductors Volume 2: Novel Superconductors

(K.-H. Bennemann and J. B. Ketterson, ed., Springer, Berlin, 2008).

³ P. Thalmeier, and G. Zwicknagl, *Unconventional Superconductivity and Magnetism in Lanthanide and Actinide Intermetallic Compounds*, Handbook of the Physics and

- Chemistry of Rare Earths Vol. 34 (North-Holland, Amsterdam, 2005).
- ⁴ D. J. Scalapino, Rev. Mod. Phys. **84**, 1383 (2012).
 - ⁵ G. R. Stewart, Adv. Phys. **66**, 75 (2017).
 - ⁶ B. Keimer, S. A. Kivelson, M. R. Norman, S. Uchida, and J. Zaanen, Nature **518**, 179 (2015).
 - ⁷ P.J. Hirschfeld, M.M. Korshunov, and I.I. Mazin, Rep. Prog. Phys. **74**, 124508 (2011).
 - ⁸ S. Onari and H. Kontani, *Iron-Based Superconductivity* (P.D. Johnson, G. Xu, and W.-G. Yin, ed., Springer-Verlag Berlin and Heidelberg GmbH & Co. K, 2015)
 - ⁹ N. D. Mathur, F. M. Grosche, S. R. Julian, I. R. Walker, D. M. Freye, R. K. W. Haselwimmer, and G. G. Lonzarich, Nature **394**, 39 (1998).
 - ¹⁰ T. Shibauchi, A. Carrington, and Y. Matsuda, Annu. Rev. Condens. Matter Phys. **5**, 113 (2014).
 - ¹¹ K. Hashimoto *et al.*, Science **336**, 1554 (2012).
 - ¹² G. Knebel, D. Aoki, J.-P. Brison and J. Flouquet, J. Phys. Soc. Jpn. **77**, 114704 (2008).
 - ¹³ T. Park, F. Ronning, H. Q. Yuan, M. B. Salamon, R. Movshovich, J. L. Sarrao and J. D. Thompson, Nature **440**, 65 (2006).
 - ¹⁴ H. Shishido, T. Shibauchi, K. Yasu, T. Kato, H. Kontani, T. Terashima, and Y. Matsuda, Science **327**, 980 (2010).
 - ¹⁵ M. Shimozaawa, S. K. Goh, T. Shibauchi, and Y. Matsuda, Rep. Prog. Phys. **79**, 074503 (2016).
 - ¹⁶ C. Petrovic, P. G. Pagliuso, M. F. Hundley, R. Movshovich, J. L. Sarrao, J. D. Thompson, Z. Fisk, and P. Monthoux, J. Phys. Condens. Matter **13**, L337 (2001).
 - ¹⁷ Y. Mizukami, H. Shishido, T. Shibauchi, M. Shimozaawa, S. Yasumoto, D. Watanabe, M. Yamashita, H. Ikeda, T. Terashima, H. Kontani, and Y. Matsuda, Nat. Phys. **7**, 849 (2011).
 - ¹⁸ S. K. Goh, Y. Mizukami, H. Shishido, D. Watanabe, S. Yasumoto, M. Shimozaawa, M. Yamashita, T. Terashima, Y. Yanase, T. Shibauchi, A. I. Buzdin, and Y. Matsuda, Phys. Rev. Lett. **109**, 157006 (2012).
 - ¹⁹ M. Shimozaawa, S. K. Goh, R. Endo, R. Kobayashi, T. Watashige, Y. Mizukami, H. Ikeda, H. Shishido, Y. Yanase, T. Terashima, T. Shibauchi, and Y. Matsuda, Phys. Rev. Lett. **112**, 156404 (2014).
 - ²⁰ T. Ishii, R. Toda, Y. Hanaoka, Y. Tokiwa, M. Shimozaawa, Y. Kasahara, R. Endo, T. Terashima, A. H. Nevidomskyy, T. Shibauchi, and Y. Matsuda, Phys. Rev. Lett. **116**, 206401 (2016).
 - ²¹ M. Naritsuka, T. Ishii, S. Miyake, Y. Tokiwa, R. Toda, M. Shimozaawa, T. Terashima, T. Shibauchi, Y. Matsuda, and Y. Kasahara, Phys. Rev. B **96**, 174512 (2017).
 - ²² M. Naritsuka, P. F. S. Rosa, Y. Luo, Y. Kasahara, Y. Tokiwa, T. Ishii, S. Miyake, T. Terashima, T. Shibauchi, F. Ronning, J. D. Thompson, and Y. Matsuda, Phys. Rev. Lett. **120**, 187002 (2018).
 - ²³ R. Settai, T. Takeuchi, and Y. Onuki, J. Phys. Soc. Jpn. **76**, 051003 (2007).
 - ²⁴ Y. Kawasaki, S. Kawasaki, M. Yashima, T. Mito, G. Zheng, Y. Kitaoka, H. Shishido, R. Settai, Y. Haga, and Y. Onuki, J. Phys. Soc. Jpn. **72**, 2308 (2003).
 - ²⁵ S. Raymond and G. Lapertot, Phys. Rev. Lett. **115**, 037001 (2015).
 - ²⁶ K. Izawa, H. Yamaguchi, Y. Matsuda, H. Shishido, R. Settai, and Y. Onuki, Phys. Rev. Lett. **87**, 057002 (2001).
 - ²⁷ K. An, T. Sakakibara, R. Settai, Y. Onuki, M. Hiragi, M. Ichioka, and K. Machida, Phys. Rev. Lett. **104**, 037002 (2010).
 - ²⁸ Y. Matsuda, K. Izawa, and I. Vekhter, J. Phys.: Condens. Matter **18**, R705 (2006).
 - ²⁹ C. Stock, C. Broholm, J. Hudis, H. J. Kang, and C. Petrovic, Phys. Rev. Lett. **100**, 087001 (2008).
 - ³⁰ B. B. Zhou, S. Misra, E. H. da Silva Neto, P. Aynajian, R. E. Baumbach, J. D. Thompson, E. D. Bauer, and A. Yazdani, Nat. Phys. **9**, 474 (2013).
 - ³¹ M. P. Allan, F. Massee, D. K. Morr, J. Van Dyke, a. W. Rost, a. P. Mackenzie, C. Petrovic, and J. C. Davis, Nat. Phys. **9**, 468 (2013).
 - ³² T. Tayama, A. Harita, T. Sakakibara, Y. Haga, H. Shishido, R. Settai, and Y. Onuki, Phys. Rev. B **65**, 180504(R) (2002).
 - ³³ A. Bianchi, R. Movshovich, N. Oeschler, P. Gegenwart, F. Steglich, J. D. Thompson, P. G. Pagliuso, and J. L. Sarrao, Phys. Rev. Lett. **89**, 137002 (2002).
 - ³⁴ Y. Matsuda and H. Shimahara, J. Phys. Soc. Jpn **76**, 051005 (2007).
 - ³⁵ V. A. Sidorov, M. Nicklas, P. G. Pagliuso, J. L. Sarrao, Y. Bang, A. V. Balatsky, and J. D. Thompson, Phys. Rev. Lett. **89**, 157004 (2002).
 - ³⁶ Y. Nakajima, H. Shishido, H. Nakai, T. Shibauchi, K. Behnia, K. Izawa, M. Hedo, Y. Uwatoko, T. Matsumoto, R. Settai, Y. Onuki, H. Kontani, and Y. Matsuda, J. Phys. Soc. Jpn. **76**, 024703 (2007).
 - ³⁷ J. L. Sarro and J. D. Thompspon, J. Phys Soc. Jpn. **76**, 051013 (2007).
 - ³⁸ T. Yamanaka, M. Shimozaawa, R. Endo, Y. Mizukami, H. Shishido, T. Terashima, T. Shibauchi, Y. Matsuda, and K. Ishida, Phys. Rev. B **92**, 241105(R) (2015).
 - ³⁹ D. Maruyama, M. Sigrist, and Y. Yanase, J. Phys. Soc. Jpn. **81**, 034702 (2012).
 - ⁴⁰ G. Nakamine, T. Yamanaka, S. Kitagawa, M. Naritsuka, T. Ishii, T. Shibauchi, T. Terashima, Y. Kasahara, Y. Matsuda, and K. Ishida, Phys. Rev. B **99**, 081115(R) (2019).
 - ⁴¹ A. Benoit, J. X. Boucherle, P. Convert, J. Flouquet, J. Pellau, and J. Schweizer, Solid State Commun. **34**, 293 (1980).
 - ⁴² G. Knebel, D. Braithwaite, P. C. Canfield, G. Lapertot, and J. Flouquet, Phys. Rev. B **65**, 024425 (2001).
 - ⁴³ N. R. Werthamer, E. Helfand, and P. C. Hohenberg, Phys. Rev. **147**, 295 (1966).
 - ⁴⁴ E. Bauer and M. Sigrist, *Non-Centrosymmetric Superconductors: Introduction and Overview, Lecture Notes in Physics* (Springer-Verlag, Berlin, Heidelberg, 2012).
 - ⁴⁵ S. Fujimoto, J. Phys. Soc. Jpn. **76**, 051008 (2007).
 - ⁴⁶ G. Knebel, M.-A. Méasson, B. Salce, D. Aoki, D. Braithwaite, J. P. Brison, and J. Flauquet, J. Phys.: Condens. Matter **16**, 8905 (2004).
 - ⁴⁷ W. Bao, P. G. Pagliuso, J. L. Sarrao, J. D. Thompson, Z. Fisk, J. W. Lynn, and R. W. Erwin, Phys. Rev. B **62**, R14621 (2000).
 - ⁴⁸ T. Park, E.D. Bauer, and J.D. Thompson, Phys. Rev. Lett. **101**, 177002 (2008).